Acoustic plasmons and cuprate superconductivity

Y. Ishii
Department of Material Science, Himeji Institute of Technology, Kamigori, Hyogo 678-12, Japan

J. Ruvalds*
Physics Department, Stanford University, Stanford, California 94305
(Received 24 August 1992; revised manuscript received 1 February 1993)

The plasmon response is analyzed for a tight-binding model of two energy bands. The majority charge carriers originate from the Cu-O planes with copper orbitals of $d_{x^2-y^2}$ symmetry hybridized with the oxygen p states. The second band is more localized and yields low-energy acoustic plasmons that are well defined over a wide momentum range for appropriate positions of the Fermi energy E_F. The use of bandwidths comparable to band-structure computations for $YBa_2Cu_3O_7$ yields a maximum energy $\Theta \simeq 0.2$ eV for the minority hole plasmon, which is a candidate for mediating superconducting pairing of the majority electrons. The transition temperature T_c is shown to correlate with the prefactor Θ as a function of E_F in a weak-coupling analysis. If removal of oxygen raises E_F, the corresponding decrease of Θ would be compatible with the observed drop in T_c for $YBa_2Cu_3O_{7-\delta}$. The calculated structure factor reveals narrow acoustic plasmon peaks that should be accessible to electron-loss probes. Threshold structure in the electronic density of states for the narrower band may be related to observed Knight-shift variations.

I. INTRODUCTION

Six years after the discovery of high-temperature superconducting oxides,[1,2] the superconducting mechanism remains an open challenge. One mystery surrounding these discoveries is the sensitivity of the transition temperature T_c to the alloy composition, including the influence of the oxygen concentration.

Proposals for the superconductivity in these oxides are constrained by a variety of experimental facts which have been reviewed by Little.[3] Flux quantization and Josephson tunneling data provide convincing evidence that the charge carriers are pairs extending over a coherence length of the order ~ 38 Å in the Cu-O planes, although the origin of the pairing interaction is not established.

A possible source of the charge-carrier pairing in the oxides is an electronic excitation extending to an energy Θ higher than the phonon regime, to roughly $\Theta \simeq 0.1-0.5$ eV. Exchange of such an excitation may bind pairs and yield a superconducting transition temperature T_c of the form

$$T_C \simeq \Theta \exp\left[-\frac{1+\lambda}{\lambda-\mu^*}\right], \tag{1}$$

where λ is the effective pairing interaction and μ^* is the reduced Coulomb repulsion between electrons defined as

$$\mu^* = \frac{\mu}{1+\mu \ln(E_F/\Theta)}, \tag{2}$$

where μ is the screened Coulomb repulsion. The allure of electronic modes is related to their potentially high-energy values with $\Theta \geq 3000$ K, which promise to raise T_c much higher than the BCS phonon mechanism whose corresponding Debye temperatures are usually much smaller, say , $\Theta_D < 300$ K.

However, the choice of an appropriate excitation for the mediation of electron pairing is limited. For example, ordinary plasmons with $\Theta \sim 5$ eV in alkali metals clearly provide no superconducting benefit to these normal metals. This type of situation is noted for strong Coulomb repulsion between electrons which cannot be overcome by exchange of a high-energy mode. Thus the characterization and physical origin of a boson mode in an appropriate energy range is vital to ascertain its prospects for high-temperature superconductivity.

Our goal is to examine a model of the electronic structure of the cuprates which is based on two tight-binding bands near the Fermi energy. Screening of the narrower band charges by majority electrons in a broader band may generate acoustic plasmon modes of the variety originally proposed by Pines.[4] Enhancement of superconducting electron pairing by exchange of such modes was suggested by Englert[5] and demonstrated by numerical calculations of Garland.[6] Formulations[7] analogous to ion screening in metals establish guidelines for the formation of low-energy plasmons that need to avoid severe Landau damping. However, the lack of definitive experimental evidence for this type of electronic excitation has hampered theoretical attempts[8] to identify materials that may be suitable prospects for these elusive acoustic excitations.

The nearly two-dimensional (2D) character of the electron dynamics in the Cu-O planes may create plasmon features that are particularly relevant to tight-binding bands. Previous calculations of the electron response in the effective-mass approximation demonstrate the existence of an acoustic plasmon branch[9] in a single charge layer by virtue of the 2D screened Coulomb potential,

and such modes have been observed by light-scattering spectroscopy.[10] Kresin[11] claimed that a single-component plasmon branch of low frequency could couple strongly to phonons and thereby enhance electron pairing. However, Mahan and Wu[12] calculated the coupling caused by a single plasmon branch with parameters suitable for oxides and concluded that exchanging such a mode alone does not enhance T_c.

Multilayers alter the screened Coulomb potential and hence generate plasmon branches which may have acoustic dispersion in a given propagation direction and a more familiar bulklike optic plasmon otherwise.[13] These characteristic modes have been seen by light scattering from GaAs superlattices.[14]

Lower dimensionality bolsters the prospects of forming a particular variety of two-component plasmons because Landau damping of the lower energy branch can be minimized in some regions of phase space that are sensitive to the position of the narrow energy band. Analytic solutions[9] of the response for two bands with different effective masses in 2D were found[15] to yield an acoustic branch whose existence was surmised to correlate with the superconducting transition temperature of $La_{2-x}Sr_xCuO_4$ in the metallic regime.

Canright and Vignale[16] have reported important limitations on two-component plasmas based on effective-mass models. They approximated vertex corrections by local-field factors that neglect the frequency variation of the particle-hole scattering kernel in order to achieve the summation of a diagram series. Then, using parametrized forms for the renormalized Coulomb coupling, they calculated the acoustic plasmon energy and showed that these corrections could shift the mode substantially and cause it to become overdamped in some cases. Hence the limited phase space for the acoustic branch reduces its effectiveness[16] in mediating electron pairing in a 2D electron gas as well as in the corresponding[17] 3D example.

The present work investigates the prospects for creating a well-defined acoustic plasmon mode throughout a wide momentum region by means of tight-binding energy bands that are designed to resemble the situation in superconducting cuprates. The nearly two-dimensional planar structure of the copper oxide planes is therefore a key input in our analysis. Our results in the random phase approximation (RPA) demonstrate certain advantages of the cuprate electronic structure for creating acoustic plasmons with a relatively small damping throughout the Brillouin zone. These encouraging features may stimulate future studies of self-energy and vertex corrections in a tight-binding context.

Reliable quantitative estimates of superconducting transition temperatures arising from electronic sources are difficult to obtain in any event. Even the case of a single-component electron gas requires corrections[18] beyond the RPA, and electron pairing by exchange of acoustic plasmons is also beset by uncertainties of higher-order processes.[18] Vertex corrections to the electron interactions originating from electronic modes are rather sensitive to the symmetry and localization of the wave functions.[19] These considerations also apply to exciton mechanisms of the type originally proposed by Little.[20]

Section II contains the energy-band model and results for the dielectric function. Explicit numerical calculations of the plasmon dispersion and structure factor are in Sec. III. Indirect evidence for the conditions needed to form appropriate acoustic plasmons can be related to the density of electronic states obtained in Sec. IV. The latter results may be related to anomalous Knight-shift data of the cuprates. Finally, conclusions of the present study are in Sec. V.

II. ENERGY-BAND MODEL

Band-structure calculations for cuprates have now received strong support from photoemission[21,22] as well as de Haas-van Alphen[23] experiments that map key features of the Fermi surface in the metallic phases. By contrast, the cuprate transition to an insulating state at a critical oxygen content is beyond the reach of band calculations and remains theoretically unresolved.

Calculations[24–28] of electronic structures in $YBa_2Cu_3O_7$ provide the motivation for the tight-binding model used here. A nearly half-filled majority-carrier band in two dimensions is chosen as

$$E_l = l_1[\cos(a_x k_x)+\cos(a_y k_y)] , \tag{3}$$

with a bandwidth $4l_1 \simeq 5.0$ eV. The heavy-mass band is assumed to be given by a simple cosine band as

$$E_h(k) = t_1\cos(k_x a_x)+t_2\cos(k_y a_y)+E_h(0) , \tag{4}$$

where a_x and a_y are the lattice constants of the Cu-O plane. Our model band structure is shown in Fig. 1.

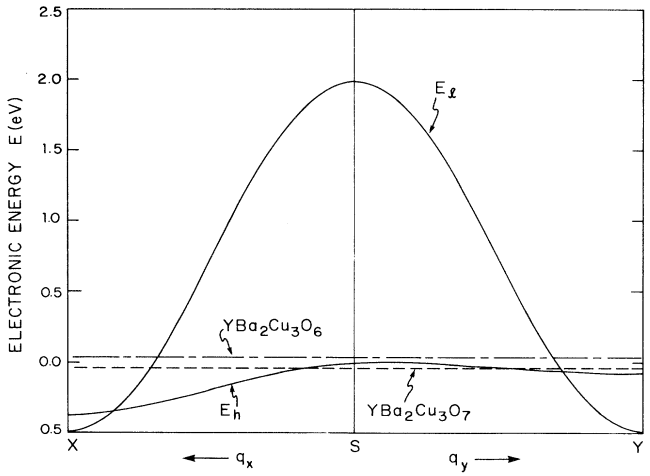

FIG. 1. Energy-band model used in our calculations. The position of the Fermi energy E_F intersects both tight-binding bands in the optimum superconducting case $YBa_2Cu_3O_7$. The bandwidths are $l_1=1.25$ eV, $t_1=0.2$ eV, $t_2=0.04$ eV, and $a_x=a_y=3.9$ Å. As oxygen is removed, E_F moves up and reaches the top of the narrow E_h band for $x \simeq 6.5$ providing that E_F moves linearly between the values given by band structures for $x=7$ (Ref. 24) and $x=6$ (Ref. 25).

The possible formation of a low-energy plasmon mode originating from the partially filled E_h band in the case of YBa_2CuO_7 will be strongly influenced by the screening of the Coulomb potential by the lighter band E_l charges. Removal of oxygen raises the Fermi energy above the E_h band, thus eliminating the secondary plasmon mode. The relative bandwidths l_1, t_1, and t_2 are similar to the band computation results. However, the position of the narrow E_h band must ultimately rely on experiment to establish the offset $E_h(0)$, which we take as 0.26 eV. Nevertheless, it is interesting to note that the raising of the Fermi energy E_F by depleting the oxygen content is compatible with computations for $YBa_2Cu_3O_6$.[25]

The Fermi surface corresponding to band-structure calculations is shown in Fig. 2, with the shaded area emphasizing the partially filled hole pocket near the symmetry point S which is a key element of the present analysis. A small increase in the Fermi energy will shrink and ultimately eliminate this small orbit, by oxygen depletion, for example. Photoemission data[21] (squares in Fig. 2) provide evidence for the large orbits corresponding to the nearly half-filled band as well as the small hole pocket. The de Haas-van Alphen experiments[23] on $YBa_2Cu_3O_7$ confirm the area of the small (shaded) Fermi-surface section.

The dielectric function for the band is given by

$$\epsilon_j(q,\omega)=1+V_q\chi_j(q,\omega) \tag{5}$$

within the random-phase approximation (RPA) where $V_q=2\pi e^2/q$ in two dimensions and the dynamical polarizability is calculated using

$$\Delta_j(\mathbf{k}_1\mathbf{q})=E_j(\mathbf{k}+\mathbf{q}/2)-E_j(\mathbf{k}-\mathbf{q}/2)\ , \tag{6a}$$

and the standard expression

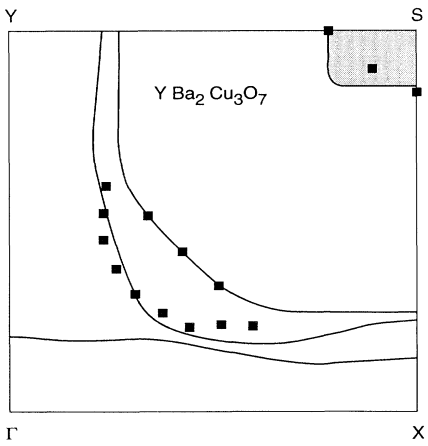

FIG. 2. Composite sketch of the Fermi surfaces of $YBa_2Cu_3O_7$ obtained from the band-structure calculations of Refs. 24–28. Squares indicate photoemission data points from Ref. 21, and the shaded region represents the orbit area measured in de Haas-van Alphen experiments of Ref. 23. Symmetry points Γ, X, Y, and S are defined in Ref. 27.

$$\chi_j(\mathbf{q},\omega)=2\sum_k f_{k-q/2}(1-f_{k+q/2}) \times\left[\frac{1}{\omega+\Delta_j(\mathbf{k},\mathbf{q})-i\delta}-\frac{1}{\omega-\Delta_j(\mathbf{k},\mathbf{q})-i\delta}\right], \tag{6b}$$

where f_k is the Fermi-Dirac function. In the energy range of interest we are justified in using the zero-temperature limit of f_k which becomes a Heaviside step function. The real part of the polarizability becomes

$$\mathrm{Re}\chi_j=-4\sum_k\frac{\Delta_j(k,q)}{\omega^2-\Delta_j^2(k,q)}f_{k-q/2}(1-f_{k+q/2})\ , \tag{7}$$

where

$$\Delta_l(k,q)=-2l_1\left[\sin(a_xk_x)\sin\left[\frac{a_xq_x}{2}\right]+\sin(a_yk_y)\sin\left[\frac{a_yq_y}{2}\right]\right] \tag{8}$$

and

$$\Delta_h(k,q)=-2t_1\sin(a_xk_x)\sin\left[\frac{a_xq_x}{2}\right]-2t_2\sin(a_yk_y)\sin\left[\frac{a_yq_y}{2}\right], \tag{9}$$

with a similar expression for the imaginary part of χ_j. For general values of q and ω, we have evaluated χ_h numerically to find the overall plasmon spectrum from the total dielectric function,

$$\epsilon_T(q,\omega)=1+V_q\chi_l(q,\omega)+V_q\chi_{hj}(q,\omega)\ . \tag{10}$$

Zeroes of the dielectric function $\epsilon_T(q,\omega)$ determine the plasmon excitation energies as a function of momentum, and the imaginary part of ϵ_T yields the damping by decay into the electron-hole continuum. Another source of plasmon damping is the electron or hole lifetime, which is limited by impurity, phonon, and electronic scattering.

Interband transitions are estimated to have a minor effect on the plasmon dispersion in the present circumstances and, therefore, are not presented here. First we calculate the plasmon spectrum for an isolated plane of electrons and then consider the further influence of interlayer coupling.

III. PLASMON DISPERSION AND DAMPING

The evaluation of the dielectric function for the tight-binding band in Eqs. (9) and (10) was performed numerically with the cutoff points for the momentum integration found by conventional techniques for the Fermi function in the zero-temperature limit. By itself, the majority hole band yields an acoustic plasmon branch by virtue of the two-dimensional character of the electron dynamics, and the dispersion relation for this plasmon mode at small q is

$$\omega_l(q)\simeq bq^{1/2}\ , \tag{11}$$

where the coefficient b is determined by the bandwidth l_1 and the carrier density. This branch is outside the electron-hole continuum, thus avoiding Landau damping up to a cutoff momentum q_c. This higher frequency majority-carrier plasmon should be relatively insensitive to small changes in the Fermi energy compared to $E_F \simeq 2.0$ eV.

The physical origin of this acoustic plasmon dispersion can be traced to the average electric field in two dimensions. Unlike the three-dimensional electron gas with $V_q^{3D}=4\pi e^2/q^2$ and its "optic" plasmon branch with a finite frequency $\omega_{pl}^2(3D)=4\pi ne^2/m^*$ in the $q=0$ limit, the 2D Coulomb $V_q^{2D}=2\pi e^2/q$ causes ω_l to vanish as q tends to zero.

Despite its "acoustic" behavior in the sense of a vanishing energy at small momentum, this majority plasmon extends to $\omega_l(q_c)\simeq E_F$, and therefore is an unlikely candidate for mediating a pairing interaction for the reasons discussed above. This type of acoustic plasmon mode has been detected experimentally in systems[10] which are not superconducting.

A surprising feature of our calculations for the majority hole band E_l is the inadequacy of the effective-mass approximation for the present two-dimensional structure. Our first attempt to fit the E_l band to the band-structure results with an effective mass $m^*\simeq m_e$ gave a reasonably good representation of the majority hole structure shown in Fig. 1, but the analytic expressions for the dielectric function yield a plasmon branch extending up to $k_B\Theta_l \simeq 20$ eV for a Fermi energy of $E_F=2.0$ eV. Unlike the three-dimensional case, the effective-mass model gives a two-dimensional acoustic plasmon which stays above the electron-hole continuum over a wide energy range and eventually becomes tangent to the continuum at a large value of Θ_l, which is an order of magnitude larger than the corresponding tight-binding results given below. In three dimensions, the effective-mass approximation yields a plasmon spectrum in better agreement with the tight-binding formulation.[29]

By using the tight-binding formula for E_l with a bandwidth $l_1=1.25$ eV we obtain a majority plasma with energy extending to roughly 4.6 eV as shown in Fig. 3, and a minority acoustic plasmon branch for parameters suitable to the electronic structure of $YBa_2Cu_3O_7$. This second branch at lower energy arises with an acoustic dispersion

$$\omega_h(\mathbf{q})\simeq c\mathbf{q}\ , \tag{12}$$

at long wavelength. The linear dispersion is a consequence of the screening of the "heavy" holes by the lighter mass carriers. Remarkably, the ω_h plasmon persists above the h-band electron-hole continuum over the entire Brillouin zone and exhibits a dispersion similar to ordinary phonons even though the plasmon energy scale is significantly higher. These calculated results differ substantially from comparable studies using an effective-mass approximation.[15]

Landau damping of the ω_h plasmon by decay into the light electron-hole continuum follows from the imaginary part of the total dielectric function ϵ_T, and is indicated by the bars on the plasmon energy dispersion in Fig. 4 for two values of the Fermi energy. The width caused by decay into the wider E_l band continuum is considerably smaller than the plasmon energy so that the particular branch exists as a well-defined excitation throughout the Brillouin zone.

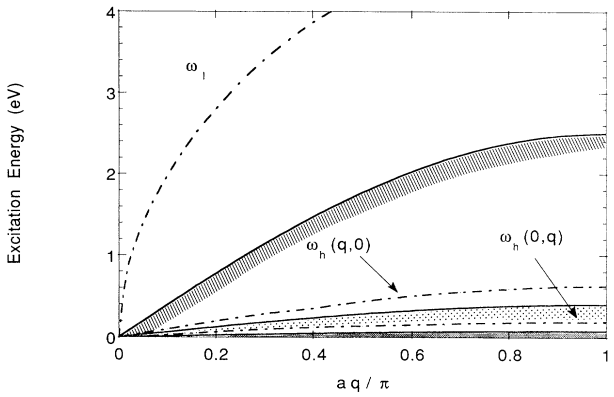

FIG. 3. The plasma spectrum calculated for the tight-binding model of a single plane. The majority holes yield a high-energy plasmon branch which is acoustic because of the two-dimensional nature of the Coulomb potential and electronic structure. This higher energy mode shifts slightly as the Fermi energy is varied. The lower acoustic plasmon branch has energy proportional to momentum at long wavelength by virtue of the screening of the Coulomb interaction, and the latter mode ω_h is a candidate for mediating electron (or hole) pairing. The shaded region represents the h-band electron-hole continuum for the two momentum directions, and the persistence of the ω_h above each corresponding continuum extends throughout the Brillouin zone in both directions.

In the long-wavelength limit, the linear dispersion of the acoustic plasmon may be deduced by expanding the dielectric function at small q as

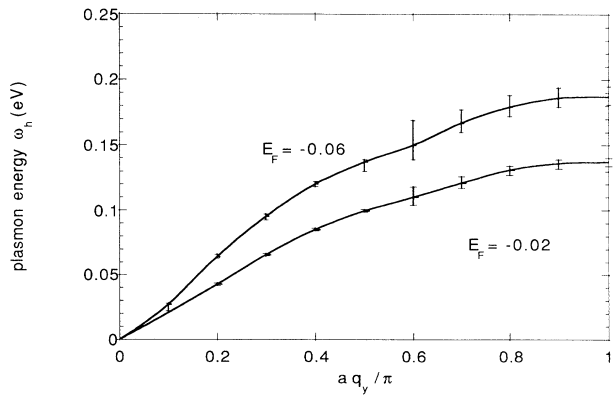

FIG. 4. Dispersion of the low-energy plasmon branch along the q_y direction for two values of the Fermi energy E_f. providing that oxygen removal from $YBa_2Cu_3O_7$ raises E_f, the softening of this mode corresponds to the observed decrease in the superconducting transition temperature T_c. The bars indicate the relatively narrow linewidths in the structure factor whose origin is the decay into the wider E_1 band electron-hole continuum.

$$\Delta_h(k,q) \simeq -t_1 a_x q_x \sin(a_x k_x) - t_2 a_y q_y \sin(a_y k_y) \quad (13)$$

and

$$f_{k-q/2}(1-f_{k+q/2}) \simeq \tfrac{1}{2}\Delta_h(k,q)\delta(E_h - E_f) , \quad (14)$$

where the zero-temperature limit of the Fermi-Dirac function has been taken. Then the real part of the susceptibility is

$$\mathrm{Re}\chi_h \simeq -2\sum_k \frac{\Delta_h^2(k,q)}{\omega^2}\delta(E_h - E_F) . \quad (15)$$

Performing the k_y integration, we obtain

$$\mathrm{Re}\chi_h = -\frac{2t_1(qa_x)^2}{\pi^2\omega^2}(F_x\cos^2\theta + F_y\sin^2\theta) , \quad (16)$$

where

$$F_x = t_1 \int_{\max(-1,(E_F-t_2)/t_1)}^{\min(1,(E_F+t_2)/t_1)} dx \left[\frac{(1-x)(x+1)}{(E_F+t_2-xt_1)(xt_1+t_2-E_F)}\right]^{1/2} , \quad (17)$$

and

$$F_y = \frac{1}{t_1}\int_{\max(-1,(E_F-t_2)/t_1)}^{\min(1,(E_F+t_2)/t_1)} dx \left[\frac{(E_F+t_2-xt_1)(xt_1+t_2-E_F)}{(1-x)(x+1)}\right]^{1/2} . \quad (18)$$

Finally we may combine this result for the narrow band E_h with the analytic static limit for the lighter band from Eq. (6) to find the final result for the lower plasmon sound velocity,

$$C \simeq (C_x^2\cos^2\theta + C_y^2\sin^2\theta)^{1/2} , \quad (19)$$

where

$$C_{\alpha=x,y} = \frac{a}{\pi}\left[\frac{2F_\alpha t_1}{N_l(0)}\right]^{1/2} . \quad (20)$$

Using representative values of $t_1 = 0.2$ eV, $t_2 = 0.04$ eV, and $1/m^* \simeq l_1 a_x^2$, we plot the two components of the plasmon sound velocity as a function of the Fermi energy in Fig. 5. For the case of $YBa_2Cu_3O_7$ with the highest T_c, we note that the slope of the acoustic plasmon mode is roughly an order of magnitude higher than a typical phonon sound velocity. As oxygen is removed, E_F is raised, and the plasmon velocity softens to a vanishing value. For $YBa_2Cu_3O_x$, with $x \lesssim 6.5$ corresponding to a filled E_h band, this lower energy plasmon ceases to exist.

A rough correlation of the observed T_c in comparison to an effective plasmon cutoff energy,

$$\Theta_h \simeq (C_x^2 + C_y^2)^{1/2} q_c , \quad (21)$$

can be achieved using the relation $T_c \propto \Theta_h$ in a weak-coupling BCS formulation from Eq. (1). Here the momentum cutoff is taken to be $(a_x)^{-1}$. Our calculated values of the plasmon cutoff are compared to T_c in Fig. 6. From this analysis we may infer that the acoustic plasmon mechanism provides a weak-coupling form of electron pairing which yields a qualitative variation of

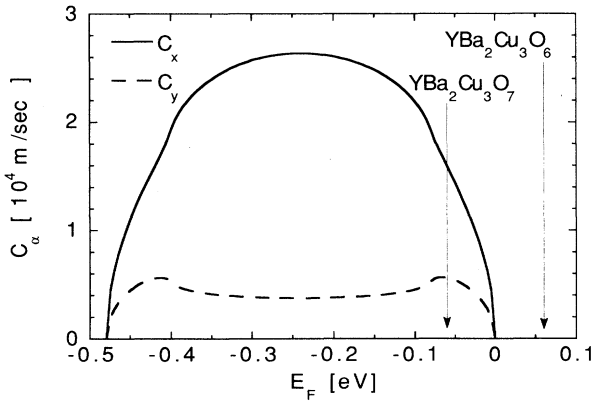

FIG. 5. Plasmon sound velocity ($\times 10^6$ m/s) as a function of the Fermi energy in eV units measured from the top of the E_h band. The anisotropy of the plasmon dispersion is seen to vary as a function of oxygen content with an overall softening of the acoustic plasmon energy as oxygen is removed from the optimum superconducting case of $YBa_2Cu_3O_7$.

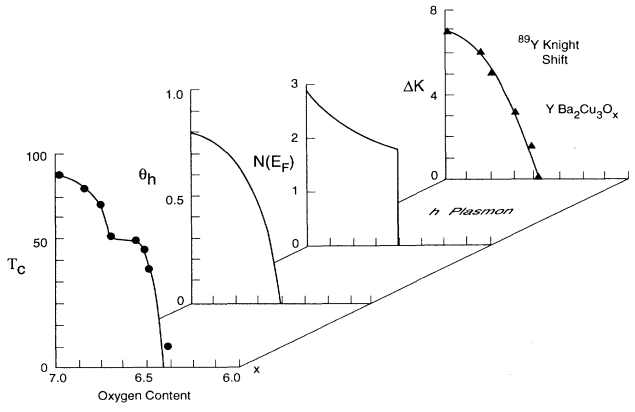

FIG. 6. Correlation of the measured superconducting transition temperature T_c (K) with the acoustic plasmon cutoff Θ_h in eV. The calculated density of states per eV/spin assumes a linear shift of E_F with oxygen content x. The Knight shift ΔK (in %) data from Ref. 30 provide evidence for a depletion of the density of states by removal of oxygen.

T_c, in accord with data on $YBa_2Cu_3O_{7-\delta}$ as a function of oxygen content. Indirect evidence for the narrow-band hole pocket density of states is provided by Knight shift data,[30] which is also shown in Fig. 6.

The electronic-structure factor is given by

$$S(q,\omega)=\frac{1}{\pi}\mathrm{Im}\frac{-1}{\epsilon_T(q,\omega)} , \tag{22}$$

where the total dielectric function ϵ_T is defined in Eq. (11). It is sampled directly by electron-loss scattering measurements which, in principle, provide the ideal direct probe of the plasmon excitations. Our computed structure factor for $YBa_2Cu_3O_7$ is shown in Figs. 7 and 8, in the range where the low-energy plasmon dominates the structure. The narrow widths of the acoustic plasmon peaks at various momentum values are due to the small Landau damping of the lower plasmon branch by decay into the lighter electron-hole continuum. Electron-loss spectroscopy evidence for the low-energy plasmon has been recently discovered by Demuth.[31]

Additional broadening caused by Umklapp channels is expected to be important, especially at small momenta $aq \lesssim 0.5$.

Impurity scattering modifies the acoustic plasmon mode in a very long wavelength region. The motion of electrons with different energies correlates through impurity scattering. This correlation modifies the polarizability in a long-wavelength and low-frequency region as[32]

$$\chi_l(q,\omega)=N_l(E_F)\frac{Dq_2}{Dq^2-i\omega} , \tag{23}$$

where $D=v_F^2\tau/2$ is the diffusion constant with the electron lifetime τ. Then the acoustic plasmon mode becomes overdamped and diffusive if $\omega_h > Dq^2$ or $q < c/D$, as in Eq. (12).

Assuming a carrier density of 1 electron per

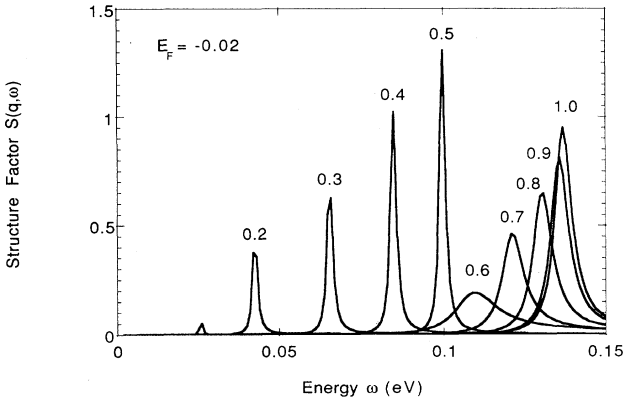

FIG. 7. Structure factor for the acoustic plasmon response at assorted momentum values along the q_y direction as a function of energy for a Fermi energy appropriate to $YBa_2Cu_3O_7$. The majority plasmon mode yields only a smooth background in this low-energy regime, and the peak structure is due to the lower energy band corresponding to the narrower band E_h. The narrow linewidths reflect the small Landau damping of the low-energy mode by decay into the l-band electron-hole continuum.

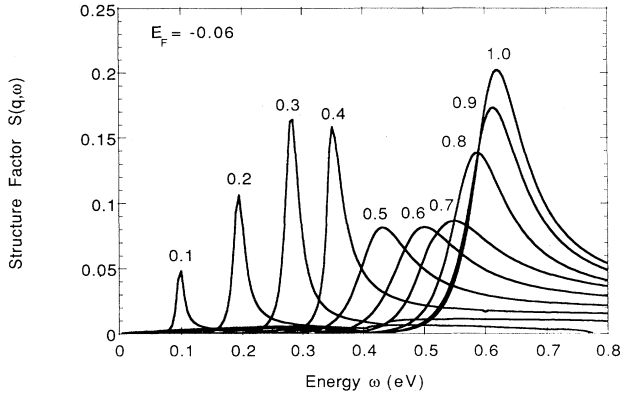

FIG. 8. Structure factor as a function of energy for momentum values parallel to the q_x axis for the parameters appropriate to $YBa_2Cu_3O_7$. The ω_h plasmon linewidths assure well-defined excitations here as well as in Fig. 7.

$(3.9)^2\times 11.7$ Å^3 unit cell, $E_F \simeq 2.0$ eV, and a resistivity of 100 $\mu\Omega$ cm, we estimate $D \simeq 10$, which implies that the ω_h branch suffers from impurity broadening only at very low momenta $q \ll \pi/a$.

Interlayer Coulomb interactions between charges on nearby Cu-O planes have a particularly strong influence in the long-wavelength limit.[13] To illustrate possible changes in the dielectric screening of nearby planes, we consider the screened Coulomb potential for a series of identical planes which are separated by a distance d. Denoting q as the momentum within the plane and k as the perpendicular component of the momentum, the Fourier transform of the Coulomb potential becomes

$$V(q,k)=\frac{2\pi de^2}{q}\frac{\sinh(qd)}{\cosh(qd)-\cos(kd)} . \tag{24}$$

In the $d\to\infty$ limit, the V_q reduces to the single plane result used above, whereas in the $d\to 0$ limit an ordinary three-dimensional electron potential results.

The plasmon spectrum follows from the total dielectric function of Eq. (5) using the modified $V(q,k)$ and presuming negligible band dispersion perpendicular to the planes. Our calculated interlayer plasmon spectrum is shown in Fig. 9. The majority hole plasmon splits into branches designated by the perpendicular momentum k. When the electron oscillations in adjacent planes are out of phase, i.e., $k=\pi/d$, the plasmon dispersion is close to the ordinary single plane result at large momenta $qd > 1$. However, the initial slope of the ($kd=\pi$ case) multilayer acoustic plasmon at long wavelengths is given by $\omega_l \simeq sq$ with $s=(dm_0/2l_1a_x^2a_0)^{1/2}v_{lF}$, where a_0 is the Bohr radius, m_0 is the free-electron mass, and v_{lF} is the Fermi velocity for the majority charge carriers from the E_l band. In-phase oscillation yield a finite optical frequency at $q \simeq 0$ as seen in the curve for $k=0$, where the computed value of the optical plasmon gap near 2.7 eV in the tight-binding model is consistent with the conventional effective-mass plasma frequency $\omega_l^2(0,0)=4\pi ne^2/m_0$ for $n=1$ electron per $(3.9)^2\times 11.7$ Å^3 unit cell. At higher momentum, these branches, as well as intermediate k

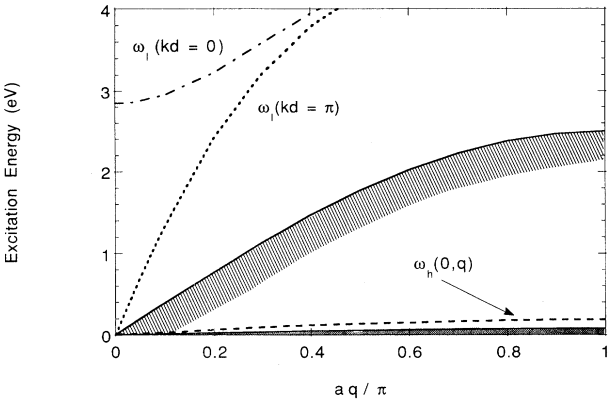

FIG. 9. Plasmon spectrum for the two-band model including the influence of interlayer Coulomb coupling. The higher energy branch ω_l splits into an acoustic dispersion for a perpendicular momentum $k=\pi/d$, and exhibits an optic mode with finite frequency at long wavelengths when $k=0$. The acoustic plasmon branch ω_h at lower energy is shifted only slightly by the interlayer coupling with $d=11.7$ Å. The shaded region shows the narrow-band electron-hole continuum along the q_y direction which remains below the w_h plasmon branch. The Landau damping by the wider E_1 band continuum (dashed region) is small enough to assure well-defined ω_h plasmon branches whose widths are apparent in the calculated structure factors in Figs. 7 and 8.

branches not shown here, blend into a single plasmon which persists above the electron-hole continuum over the entire Brillouin zone.

Interlayer interactions have a less pronounced effect on the lower plasmon branch ω_h as seen in Fig. 9. Physically these particular modes arise from the strong screening by the majority holes and, thus, the screened potential experienced by the more localized E_h states at low frequency is modified very little by adjacent layers. There are small shifts in the ω_h plasmon sound velocity, which nevertheless allow this branch to exist as a well-defined excitation split off from the heavy-mass electron-hole continuum.

Other formulations[33] of the multilayer cuprate plane and chain system have proposed a source of additional acoustic plasmon modes in the context of an effective-mass approximation with emphasis on local-field corrections to the dielectric function. Extensions of the formalism to obtain specific plasmon structure may reveal favorable ingredients for superconductivity. By the same token, it may be worthwhile to examine many-body corrections beyond the RPA analysis in the case of tight-binding models.

Measurements of the infrared reflectivity in ordinary metals reveal a sharp dip near the plasma frequency. By contrast, this long-wavelength spectroscopy reveals a nearly linear decrease of the reflectivity as a function of frequency in the cuprates, which has been interpreted in terms of an unconventional frequency-dependent quasiparticle damping. A theory[34] based on Fermi-surface nesting and its influence on electron-electron scattering provides a physical origin for the non-Drude reflectivity curvature and reveals a plasmon frequency that is compatible with the present calculations when a measured background dielectric function is included for optical data on $YBa_2Cu_3O_7$ (Ref. 35) as well as $Bi_2Sr_2CaCu_2O_8$ (Ref. 36). Nested Fermi-surface sections are evident for the large orbits of $YBa_2Cu_3O_7$ in Fig. 2.

Electron-loss experiments[37] confirm the unconventional shape of the calculated[34] structure factor in $Bi_2Sr_2CaCu_2O_8$ at small momenta with the normalized plasmon peak near 1 eV. In addition, the theoretical conductivity and structure factor satisfy the f-sum rules[37] required by particle conservation. Given a background $\epsilon_\infty \sim 5$, the optical and reflectivity data indicate an unrenormalized plasma frequency $\omega_{\rm pl} \sim 3$ eV in various metallic cuprates in the context of the above analysis with frequency-dependent damping. This value of $\omega_{\rm pl}$ is compatible with band-structure results,[27] and the value of 2.7 eV computed for the present model.

Hall-effect measurements will sample competing contributions from the charges in the two bands considered here, so that the magnitude and sign of the Hall coefficient R_H will be sensitive to the carrier mobilities and the Fermi-surface topology which may produce an unusual variation of R_H as a function of temperature and alloy composition even though the optical plasma frequency remains relatively unaffected.[32]

IV. DENSITY OF STATES

As the Fermi energy passes into the localized energy band E_h in our model, there is a threshold for a sharp increase in the density of states $N(E_F)$ as a consequence of the two-dimensional structure. For the light hole band in an effective-mass approximation in two dimensions, the density of states is a constant,

$$N_l(E)=\frac{m^*}{\pi} . \tag{25}$$

Near the Fermi energy, the majority-carrier tight-binding band E_l yields a relatively constant $N_l(E)$ with the correspondence $1/m^* \simeq l_1 a_x^2$. The Fermi energy is not adjacent to a Van Hove singularity in the present model, which is tailored to resemble the band-structure results. For the narrower tight-binding band, we find

$$N_h(E)=\frac{4}{\pi^2}[(t_1+t_2)^2-Z^2]^{-1/2} \times K\left[\left[\frac{4t_1t_2}{(t_1+t_2)^2-Z^2}\right]^{1/2}\right], \quad \text{for } |Z|<|t_1-t_2| , \tag{26a}$$

$$N_h(E)=\frac{4}{\pi^2}(4t_1t_2)^{-1/2}K\left[\left[\frac{(t_1+t_2)^2-Z^2}{4t_1t_2}\right]^{1/2}\right], \quad \text{for } |t_1-t_2|<|Z|<|t_1+t_2| , \tag{26b}$$

where $Z=E+t_1+t_2$ and K is the complete elliptic integral of the first kind.

These results predict a threshold in the total density of states $N_l(E)+N_h(E)$ at a Fermi energy corresponding to

an estimated oxygen content of $x \sim 0.5$. This step in $N_h(E)$ should influence probes of the static susceptibility in particular. Assuming a linear shift of E_F with oxygen context x, we obtain the variation of the heavy-hole density of states at the Fermi energy $N_h(E_F[x])$ as shown in Fig. 6.

The Orsay group[30] has discovered a large change in the Knight shift of the yttrium nucleus in $YBa_2Cu_3O_x$ which is shown in Fig. 6, in comparison to the calculated density of states, as well as the plasmon energy and measured superconducting transition temperature as a function of x. Qualitatively similar behavior is found if the Fermi energy is shifted linearly with the oxygen content. Of course, the detailed shape of the threshold in $N_h(E)$ depends on broadening caused by impurities, disorder, and overlap between chains and planes.

NMR spectra[39] of the oxygen nucleus in $YBa_2Cu_3O_{6+x}$ reveal anomalous temperature variations of the Knight shift, which become more pronounced in metallic samples at smaller x values. In an extension of the present work, the Fermi-energy placement near the density of states threshold can be shown[40] to cause the observed temperature variation of the susceptibility which is probed by the Knight shift as well as by the NMR relaxation rates. Hence the NMR measurements may provide clues to the narrow-band structure that is a key ingredient in the acoustic plasmon formation.

If an electronic excitation mediates superconducting electron pairing by itself, the ions are not involved and no isotope effect is expected. Experimentally, the observation of large shifts in the optical-phonon Raman spectrum of $YBa_2Cu_3O_7$ with the isotope ^{18}O substituted for ^{16}O provides support for the noninvolvement of these phonons in superconductivity since T_c remains essentially the same for both isotopes.[41,42]

Electrons exchanging phonons as well as acoustic plasmons may offer a mutual benefit for higher T_c. In that situation the relevant formula for T_c can be expressed as[8]

$$T_c \simeq \Theta_D \left[\frac{\Theta_{\rm pl}}{\Theta_D} \right]^{\lambda_{\rm pl}/\lambda_T} \exp\left[-\frac{1+\lambda_T}{\lambda_T-\mu^*} \right], \tag{27}$$

where $\lambda_T = \lambda_{\rm ph} + \lambda_{\rm pl}$ is the total attractive coupling between two electrons and Θ_D is the ordinary Debye temperature for phonons. In the limit of zero-coupling participation, $\lambda_{\rm ph}=0$, there is no isotope effect. By contrast, the BCS limit is $\lambda_{\rm pl}=0$, with the normal isotope effect $T_c \simeq M^{-1/2}$. In the general case, a partial isotope effect may occur with a prefactor

$$T_c \propto \theta_D^{\gamma}, \tag{28}$$

where $\gamma = \lambda_{\rm ph}/(\lambda_{\rm ph}+\lambda_{\rm pl})$. Hence the $La_{2-x}Sr_xCuO_4$ series of superconductors with a partial isotope effect may be consistent with this type of analysis.

V. CONCLUSIONS

Results of these tight-binding model calculations include the dispersion of the lower energy acoustic plasmon which allows it to exist as a well-defined excitation throughout the Brillouin zone. The curvature of the energy versus momentum is quite different than results obtained within an effective-mass approximation, and the enhanced phase-space region for the plasmon should conceivably be favorable for mediating the pairing interaction for charge carriers in the second broader energy band. The calculated structure factor reveals sharp acoustic plasmon peaks whose broadening is due to weak Landau damping by the broader band continuum.

The evolution of the acoustic plasmon energy as a function of Fermi energy is qualitatively consistent with the observed depression of the superconducting transition temperature as a function of oxygen content in $YBa_2Cu_3O_x$. Electron-loss measurements on crystals of varying oxygen content may test this prediction by methods that have provided evidence[30] for the existence of a lower energy plasmon in the $x=7$ case.

Indirect evidence for the existence of conditions that are necessary and favorable for creating the two-component plasmon structure may be surmised from measurements that are sensitive to the electronic density of states at the Fermi energy. Thus the NMR Knight-shift and oxygen relaxation rate, as well as heat-capacity and electron-tunneling data on cuprates should reveal clues to the existence of the second narrow band. Furthermore, if a superconducting energy gap opens in the wider band while leaving a finite density of states below T_c from the narrow band, the conventional analysis of properties such as the NMR rates below T_c may require consideration of the remnant normal hole component.

The incipient spin density wave (SDW) instability originating from nesting of the nearly half-filled E_l band may be influenced by the screening of the Coulomb potential by the holes in the narrow-band pocket in a subtle way. Screening in two-dimensional systems is sensitive to even a small concentration of charges.[43] Thus, the filling of the narrow-band hole pocket by decreasing oxygen content may eliminate its screening contribution and thereby lead to an abrupt enhancement of the Coulomb repulsion of electrons in the E_l band near a critical oxygen composition. In other words, the elimination of the combined screening of the Coulomb repulsion by the filled of the E_h band pocket and the opening of a SDW energy gap in the wider E_l band may lead to an insulating state with a U value much larger than the effective screened repulsion in the metallic regime.

Since the present calculations yield an improved outlook for the existence of acoustic plasmons using the standard random-phase approximation for a pair of two-dimensional tight-binding bands, they should motivate studies of self-energy and vertex corrections to these types of structures in the future.

ACKNOWLEDGMENTS

It is a pleasure to acknowledge the hospitality of the Physics Department at Harvard University, where this research was initiated. Stimulating discussions with H. Ehrenreich, B. Halperin, D. Nelson, and D. Turnbull are appreciated. One of the authors (Y.I.) appreciates il-

luminating discussions with K. Terakura and comments on the manuscript by Y. Takada. We thank Chung-Yi Lin for independent checks on our results, and we appreciate the contributions of G. Ashe, C. T. Rieck, M. Rilee, Hyun B. Shin, and A. Virosztek. Suggestions for the manuscript by C.T. Rieck have been especially helpful. This research was supported by the U.S. Department of Energy Grant No. DE-FG05-84ER45113.

*Permanent address: University of Virginia, Charlottesville, VA 22901.

[1]J. G. Bednorz and K. A. Müller, Z. Phys. B **64**, 189 (1986).
[2]M. K. Wu, J. R. Ashburn, C. J. Torng, P. H. Hor, R. L. Meng, L. Gas, Z. J. Huang, Y. Q. Wang, and C. W. Chu, Phys. Rev. Lett. **58**, 908 (1987).
[3]W. A. Little, Science **242**, 1390 (1988).
[4]D. Pines, J. Phys. **34**, 1379 (1956); D. Pines, and P. Nozières, Phys. Rev. **109**, 1062 (1958).
[5]F. Englert, *Proceedings of the International Conference on Semiconductor Physics* (Publishing House of the Czechoslovak Academy of Sciences, Prague, 1960), p. 34.
[6]J. W. Garland, *Proceedings of the Ninth International Conference on Low Temperature Physics* (Butterworths, London, 1963), p. 143.
[7]H. Fröhlich, J. Phys. C **1**, 544 (1968).
[8]J. Ruvalds, Adv. Phys. **30**, 677 (1981).
[9]F. Stern, Phys. Rev. Lett. **18**, 546 (1987).
[10]C. C. Grimes, Surf. Sci. **73**, 379 (1978); A. J. Dahm and W. F. Vinen, Phys. Today 43(2) (1987); R. A. Höpfel and E. Gornik, Surf. Sci. **143**, 412 (1984).
[11]V. Kresin, Phys. Rev. B **35**, 8716 (1987).
[12]G. D. Mahan and J. W. Wu, Phys. Rev. B **39**, 265 (1989).
[13]A. L. Fetter, Ann. Phys. (N.Y.) **88**, 1 (1974).
[14]R. Sooryakumar, A. Pinczuk, A. Gossard, and W. Wiegmann, Phys. Rev. B **31**, 2578 (1985).
[15]J. Ruvalds, Phys. Rev. B **35**, 8869 (1987).
[16]G. S. Canright and G. Vignale, Phys. Rev. B **39**, 2740 (1989); G. Vignale and K. S. Singwi, *ibid.* **32**, 2156 (1985).
[17]J. Ihm, M. L. Cohen, and S. F. Tuan, Phys. Rev. B **23**, 3258 (1981).
[18]H. Rietschel and L. J. Sham, Phys. Rev. B **28**, 5100 (1983); M. Grabowski and L. J. Sham, *ibid.* **29**, 6132 (1984).
[19]H. Gutfreund and W. A. Little, in *Highly Conducting One-Dimensional Solids,* edited by J. T. Devreese, R. P. Evard, and V. E. Doren (Plenum, New York, 1979), p. 305.
[20]W. A. Little, Phys. Rev. **134**, A1416 (1964).
[21]C. G. Olson *et al.,* J. Phys. Chem. Solids **52**, 1419 (1991); J. C. Campuzano *et al.,* Phys. Rev. Lett. **64**, 2308 (1990).
[22]D. S. Dessau *et al.,* Phys. Rev. Lett. **66**, 2160 (1991).
[23]C. M. Fowler, B. L. Freeman, W. L. Hilts, J. C. King, F. M. Mueller, and J. L. Smith, Phys. Rev. Lett. **68**, 534 (1992).
[24]J. Yu, S. Massida, A. J. Freeman, and D. D. Koeling, Phys. Lett. **122**, 203 (1987).
[25]F. Herman, R. V. Kasowski, and W. Y. Hsu, Phys. Rev. B **36**, 6904 (1987).
[26]L. F. Mattheiss and D. R. Hamann, Solid State Commun. **63**, 395 (1987).
[27]Reviews of band structures and their validity for cuprates are in W. E. Pickett, Rev. Mod. Phys. **61**, 689 (1989); W. E. Pickett, Science **255**, 46 (1992).
[28]O. K. Andersen, *et al.,* Physica C **185-189**, 147 (1991).
[29]A. Birnboim and H. Gutfreund, Phys. Rev. B **9**, 139 (1974).
[30]H. Alloul, P. Mendels, G. Collin, and P. Monod, Phys. Rev. Lett. **61**, 746 (1988).
[31]J. Demuth, Phys. Rev. Lett. **64**, 603 (1990).
[32]H. Fukuyama, Prog. Theor. Phys. **84**, Suppl. 47 (1985).
[33]A. Griffin, Phys. Rev. B **37**, 5943 (1988).
[34]J. Ruvalds and A. Virosztek, Phys. Rev. B **43**, 5498 (1991); A. Virosztek and J. Ruvalds, *ibid.* **42**, 4064 (1990).
[35]Z. Schlesinger *et al.,* Phys. Rev. Lett. **65**, 801 (1990).
[36]K. Kramers *et al.,* in *Electronic Properties of High Temperature Superconductors,* edited by H. Kuzmany *et al.,* Solid State Sciences Vol. 99 (Springer, Berlin, 1990), p. 260.
[37]N. Nücker *et al.,* Phys. Rev. B **39**, 12 379 (1989).
[38]A. Virosztek and J. Ruvalds, Phys. Rev. Lett. **67**, 1657 (1991); Phys. Rev. B **45**, 437 (1992). The Hall effect is discussed in J. Ruvalds and A. Virosztek, Phys. Rev. B **42**, 399 (1990).
[39]M. Takigawa *et al.,* Phys. Rev. B **43**, 247 (1991).
[40]C. T. Rieck and J. Ruvalds (unpublished).
[41]B. Batlogg *et al.,* Phys. Rev. Lett. **58**, 2333 (1987).
[42]L. C. Bourne *et al.,* Phys. Rev. Lett. **58**, 2337 (1987).
[43]P. B. Visscher and L. M. Falicov, Phys. Rev. B **3**, 2541 (1971).